Icarus 266 (2016) 134–141

Contents lists available at ScienceDirect

Icarus

journal homepage: www.journals.elsevier.com/icarus

High resolution spectroscopy of an Orionid meteor from 700 to 800 nm

M. Passas [a,*], J.M. Madiedo [b,c], F.J. Gordillo-Vázquez [a]

[a] Instituto de Astrofísica de Andalucía (IAA), CSIC, PO Box 3004, 18080 Granada, Spain
[b] Departamento de Física Atómica, Molecular y Nuclear, Facultad de Física, Universidad de Sevilla, 41012 Sevilla, Spain
[c] Facultad de Ciencias Experimentales, Universidad de Huelva, 21071 Huelva, Spain

ARTICLE INFO

Article history:
Received 17 September 2015
Revised 19 November 2015
Accepted 19 November 2015
Available online 27 November 2015

Keywords:
Spectroscopy
Meteorites
Atmospheres, chemistry
Image processing

ABSTRACT

The emission spectrum of a meteor was recorded by the GRASSP instrument during the observation of transient luminous events (TLEs) on 2014 October 16th. The spectroscopic signal was recorded in the wavelength range from 700 to 800 nm, where the emission from atmospheric oxygen and nitrogen dominated. The good spectral resolution of the spectrum (0.24 nm with 0.07 nm/pixel spectral dispersion) has allowed us to determine the physical conditions in the meteor plasma, to identify several emissions from atmospheric (N I, N II, O I) and meteoroid species (Ti I, Cr I, Fe I, Fe II, Zr I, Pd I, W I) and to estimate the upper limit of the temperature of the gaseous environment surrounding the meteoroid. Images recorded for this meteor from two different sites allowed calculating its atmospheric trajectory and the orbital parameters of the progenitor meteoroid. These data revealed that the particle belonged to the Orionid meteoroid stream.

1. Introduction

Comet 1P/Halley is the parent of both the η-Aquariid and the Orionid meteor showers. Their activity period ranges, approximately, from April 19th to May 25th, and from October 2nd to November 7th, respectively (Jenniskens, 2006). The analysis of meteor events produced by debris from this comet can provide information about the physical properties of these meteoroids and their dynamics in the atmosphere, but also about their chemical nature if spectral data are available. Thus, meteor emission spectroscopy has proven to be a fundamental technique to analyze the physical conditions in meteor plasmas and the composition of meteoroids ablating in the atmosphere (Borovicka, 1993; Jenniskens, 2007; Madiedo et al., 2013a). Meteor spectra contain contributions from the meteoroid, but also from atmospheric species. In general, most lines associated to the meteoroid are produced by Fe I, but the contributions of other neutral and singly ionized chemical elements have been also identified (Borovicka, 1993, 1994; Trigo-Rodriguez et al., 2009a; Madiedo et al., 2013b, c). Besides, bands of different molecules (such as, for instance, CN, N_2, C_2, FeO and CaO), have been also observed (Borovicka, 1993; Jenniskens et al., 2000; Madiedo, 2015).

This paper analyzes a meteor high resolution emission spectrum serendipitously recorded in the framework of a transient luminous event (TLE) observing campaign conducted during the activity period of the Orionid meteor shower in 2014. The signal was obtained in the wavelength range between 700 and 800 nm. The meteor was simultaneously imaged from two different sites in Spain, which provided the atmospheric trajectory and radiant of this event, but also the orbital elements of the meteoroid.

2. Instrumentation

The meteor observing station at Sierra Nevada, Granada, Spain, located at 2896 m above mean sea level, 37.05°N latitude and 03.38°W longitude, employs an array of five low-lux CCD video cameras (models 902H Ultimate and 902H2, manufactured by Watec Co., Japan) with the aim to determine the atmospheric trajectory of meteor events and the heliocentric orbit of the progenitor meteoroids. These devices generate analogue interlaced imagery following the PAL video standard at a rate of 25 frames per second (fps) and with a resolution of 720 × 576 pixels. Aspherical optics with focal length ranging from 6 to 25 mm are attached to these cameras. With this configuration each device monitors an area in the night sky ranging from 62 × 50 to 14 × 11 degrees. A detailed description of this station is given in Madiedo and Trigo-Rodriguez (2008). This CCD camera array operates in a fully autonomous way by means of software developed for this purpose (Madiedo, 2014). To obtain the atmospheric trajectory and radiant

* Corresponding author.
E-mail addresses: passasv@iaa.es (M. Passas), madiedo@cica.es (J.M. Madiedo), vazquez@iaa.es (F.J. Gordillo-Vázquez).

http://dx.doi.org/10.1016/j.icarus.2015.11.020
0019-1035/

Table 1
ICCD spectrograph features.

Wavelength range	700–800 nm
Spectral resolution	0.24 nm
Dispersion	0.07 nm/px
Time resolution	10 μs–30 ms
Slit size	0.10 mm × 31.37 mm
Field of view	0.03° × 6°
Frame rate	25 fps

of the meteor and the orbital elements of the progenitor meteoroid we have employed the AMALTHEA software (Trigo-Rodriguez et al., 2009b; Madiedo et al., 2013b), which follows the calculation methods described in Ceplecha (1987).

The GRanada Sprite Spectrograph and Polarimeter (GRASSP hereinafter, Fig. 1) is a ground-based polarimeter and grating spectrograph sensitive in the wavelength range between 700 and 800 nm, both installed on a remotely controlled telescope mount. It has been designed to measure simultaneously the polarization and the spectra of the light emitted from TLEs with a spectral resolution of $R = \lambda/\Delta\lambda = 2600$ ($\Delta\lambda = 0.24$ nm) measured at the central wavelength of 750 nm with a spectral dispersion of 0.07 nm/pixel.

The GRASSP intensified CCD (ICCD) slit spectrograph system main characteristics are fully described in Parra-Rojas et al. (2013) and Passas et al. (2014), although it was upgraded in 2014 July to shift the former spectral range to 700–800 nm and to improve its spectral resolution. Moreover, we upgraded the analog to digital system too and we installed a Blackmagic Design Decklink Mini Recorder board, which increases the HD format support to 1080 (V) × 1920 (H) pixels instead of 576 (V) × 720 (H) pixels we used to have. Table 1 shows the main features of GRASSP slit spectrograph.

The GRASSP instrument is also equipped with a wide field camera to discern the origin of the recorded spectrum. It consists of a Watec WAT-902H2 Ultimate with a 3005VX4 sensor 1/2″ CCD low light monochrome camera of high sensitivity similar as the meteor station cameras installed at Sierra Nevada. Its field of view is 30° (H) × 20° (V) thanks to the F/1.4 and 16 mm focal length lens it has attached.

In 2014 October 16th, the whole system was housed in an isothermal box which front face included a 80 × 80 cm^2 window with a mean transmittance of 69% in the band between 700 and 800 nm. It was located at the terrace of the 2.2 m dome of the German-Spanish Astronomical Center at Calar Alto, Sierra de Los Filabres, north of Almería (Andalucía, Southern Spain) fixed at 2168 m above mean sea level, 37.2231°N latitude and 2.5458°W longitude. The box was installed on an aluminum sloped fixed structure oriented to 45° azimuth from the north and 10° elevation in order to observe the western Mediterranean Sea zone (37–50°N; 2°W–14°E) with an elevation of 10–35° above the horizon, a region where the most TLE activity in Europe takes place.

3. Results

3.1. Atmospheric path, radiant and orbit

Fig. 2 shows a sum pixel intensity image of the meteor recorded from Calar Alto on 2014 October 16th at 01h19m40.4 ± 0.1 s UTC. The peak luminosity of the event was equivalent to a stellar magnitude of −2.5 ± 0.5. The meteor was simultaneously imaged from a meteor observing station located at Sierra Nevada.

The geographic coordinates of both recording sites are shown in Table 2. The triangulation of the atmospheric trajectory reveals that the luminous phase of the event began at 119.7 ± 0.5 km above the sea level and ended at a height of 82.8 ± 0.5 km. The inclination of this trajectory with respect to the local vertical was 48.5° ± 1.0″, and the meteoroid struck the atmosphere with an initial velocity of 68.1 ± 0.3 km s^{-1}, and no significant deceleration was observed while the meteoroid penetrated the atmosphere.

The apparent radiant was located at the equatorial coordinates $\alpha = 91.92 \pm 0.07°, \delta = 16.65 \pm 0.09°$. The main parameters of this atmospheric path are summarized in Table 3. The calculated orbital data of the progenitor meteoroid are listed in Table 4.

3.2. Emission spectrum

Five consecutive frames of the spectrum were recorded while the meteor was passing through the slit. To reduce long-slit spectroscopy data, we combined these frames in order to minimize the signal to noise ratio (SNR) by calculating the median value of each pixel. The spatial extension of the resulting spectrum is 1280 × 46 pixels, being the signal extracted from row 410 to row 455. We subtracted a combination of the bias frames from all images. Then, we applied a flat field correction, which consists of amending the inequity of the pixel sensitivity due to the intrinsic performance of the ICCD and/or the optics. To do so, we divided the bias-corrected ICCD image by the flat-field bias-corrected image. Later we calculated the sky background as the mean value between 10 frames – previously bias and flat-field corrected – corresponding to five frames immediately before and after the capture.

Once the sky background was subtracted from the bias-flat-field corrected image, we calibrated it in wavelength using Ne, Ar and Kr lamps in order to straighten the curvature of the spectrum through a specific Matlab software we have developed, by associating the pixel coordinates in the ICCD with the absolute wavelength by comparison with emission data whose absolute wavelengths are well-known.

We calculated the calibration curve of the instrument (Fig. 3, bottom) using the response of a commercial continuum lamp according to the steps defined in Fantz (2006). To do so, we divided

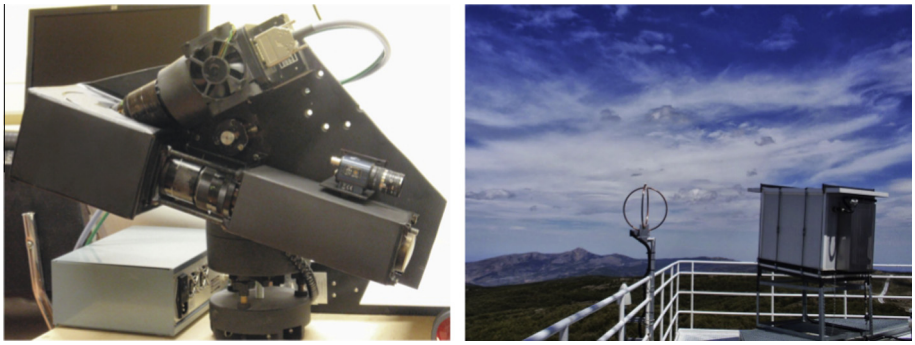

Fig. 1. GRASSP instrument 0.24 nm resolution spectrograph and housing.

Fig. 2. Sum pixel intensity image of the Orionid meteor imaged from Calar Alto.

Table 2
Geographical coordinates of the sites where the meteor analyzed in this work was imaged.

Station	Station name	Longitude (W)	Latitude (N)	Altitude (m)
1	Calar Alto (CAHA)	2°32′46″	37°13′25″	2168
2	Sierra Nevada (OSN)	3°23′05″	37°03′51″	2896

the spectral radiance of this calibrated source (Fig. 3, top) by the instrument response to the same calibrated lamp under the same calibration setting (Fig. 3, middle). The resulting curves (one for each row of the ICCD) are called the conversion factor spectral sensitivity (Fig. 3, bottom), which define the calibration curves of the instrument.

Next, we enhanced the response of the ICCD edges by flux-calibrating the corrected spectrum image. To do so, we multiplied the response of every row of the ICCD image by its corresponding conversion factor spectral sensitivity curve of GRASSP instrument. Then, we corrected the resulting spectrum by the GRASSP instrument window and the air transmittances, as in Gordillo-Vázquez et al. (2011, 2012). The air transmittance for computing the N_2 first positive system synthetic spectra between 700 nm and 800 nm was calculated using the MODTRAN code (Anderson et al., 1993) as the atmospheric transmission model. We considered a mean source altitude of 100 km and an atmospheric path length of 700 km between the source (the Orionid meteor) and the GRASSP spectrograph located in a mountain (2.2 km altitude).

Regarding that the first frame of the meteor spectrum was recorded 0.24 s after the Watec camera detection, we estimate that the altitude of the meteor at that time was 107.6 ± 0.5 km. By inspecting the resulting spectrum, and by assuming that the main contribution corresponds to line 777.194 nm of oxygen, we have identified a Doppler blueshift of 0.2 nm, which implies a projected velocity of 77 km/s ± 27 km/s (corresponding to a dispersion rate of 0.7 Å) which is consistent with the velocity derived from the analysis of the atmospheric trajectory of the event.

3.3. Identified species

Next step is to identify which species could be emitting while the meteoroid was entering the Earth's atmosphere. First, we smoothed the blueshift-corrected spectrum to increase the SNR. Then, we calculated sigma as the root mean square value (RMS) for a dark image, previously wavelength and flux calibrated. To identify the emission lines of the meteoroid spectrum we only took into account the signal over an upper limit of 2-sigma. We identified some species by modelling a synthetic spectrum combining well-known spectral lines (Kramida et al., 2014) close to the peaks over 2-sigma, previously convolved with a gaussian of a standard deviation of 0.10 nm, corresponding to a system spectral resolution of 0.24 nm. We also modelled a synthetic spectrum including the relative intensities of the atomic emission lines of O I, N I, N II for a gas temperature of 0.13788 eV (~1500 K). Then, we combined the above atomic synthetic spectra with a synthetic spectrum of the N_2 first positive system (Gordillo-Vázquez et al., 2011, 2012;

Table 3
Atmospheric trajectory and radiant data (J2000). Hb and He: beginning and ending height of the meteor, respectively; α_g, δ_g: right ascension and declination of the geocentric radiant; V_∞, V_g, V_h: observed preatmospheric, geocentric and heliocentric velocities, respectively.

H_b (km)	H_e (km)	α (°)	δ (°)	V_∞ (km s^{-1})	V_g (km s^{-1})	V_h (km s^{-1})
119.7 ± 0.5	82.8 ± 0.5	91.7 ± 0.1	16.5 ± 0.1	68.1 ± 0.3	66.9 ± 0.3	40.9 ± 0.3

Table 4
Orbital parameters of the meteoroid (J2000).

a (A.U.)	e	i (°)	ω (°)	Ω (°)	q (A.U.)	P (yr)	T_J	D_{SH}
8.7 ± 1.9	0.92 ± 0.01	165.9 ± 0.2	74.9 ± 1.0	22.40735 ± 10^{-5}	0.642 ± 0.005	25.82	−0.35 ± 0.27	0.11

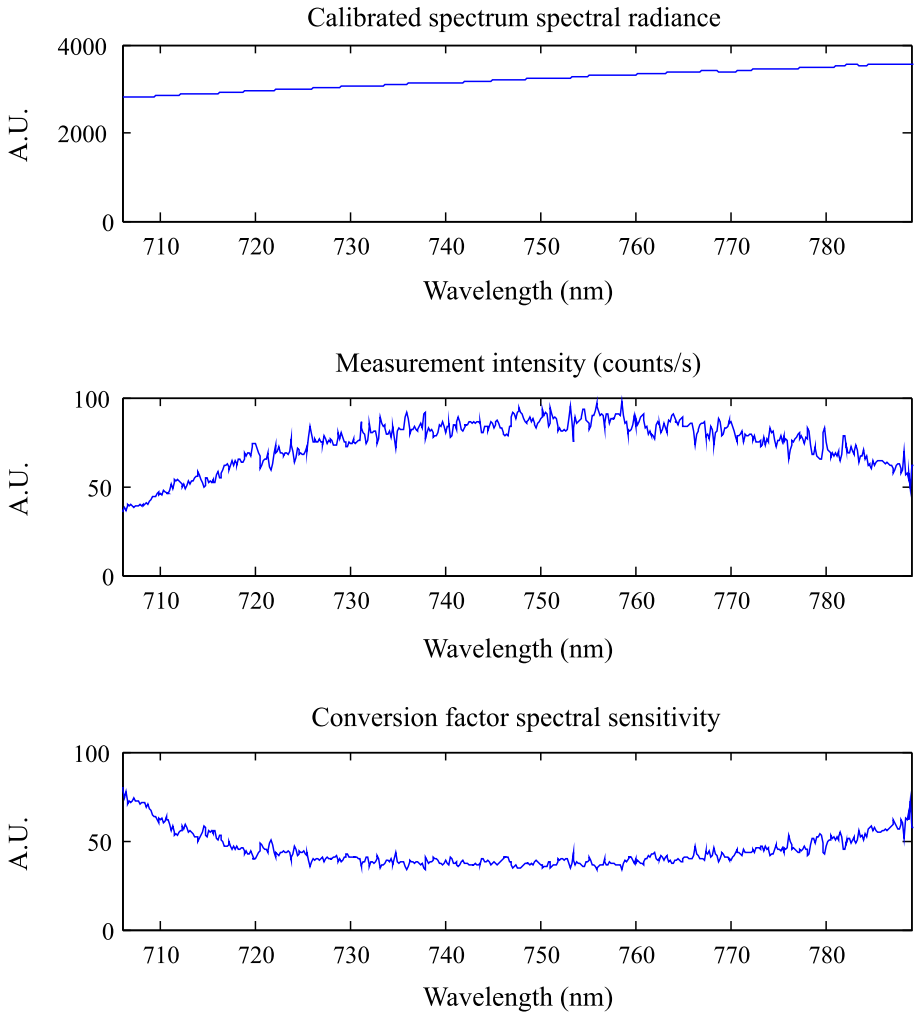

Fig. 3. Calibrated spectrum spectral radiance of a commercial lamp (top). GRASSP spectrograph response to the same commercial lamp under the same calibration settings for row number 26 (middle). Conversion factor spectral sensitivity of GRASSP instrument for row number 26 (bottom).

Parra-Rojas et al., 2013). Table 5 shows that the mean wavelength difference between measured and modelled spectra is 0.9 Å, being the intensity measured in arbitrary units (A.U.).

In order to generate the synthetic spectrum of the N_2 first positive system between 700 nm and 800 nm we have assumed Boltzmann distributions for the populations of N_2 ($B^3\Pi_g$) rotational and vibrational levels considering $T_{rot} = T_{vib} = T = 1500$ K, that is the calculated upper gas temperature limit obtained from the numerical solution of Eq. (4) below (see Section 3.4). The main contributions of the corrected spectrum over 2-sigma are listed in Table 5, where contributions over 3-sigma are bold typefaced. The contributions over 3-sigma correspond to the emissions of atmospheric N I and O I, and the contributions over 2-sigma seem to correspond to the emissions of N I, N II and O I, but also to the meteoroid-forming species Ti I, Cr I, Fe I, Fe II, Zr I, Pd I and W I. We also find coincidences with several peaks below 2-sigma when we include spectral lines of the above identified species in the range between 700 nm and 800 nm. Fig. 4 shows both synthetic and measured spectra.

3.4. Estimation of an upper limit of the gas temperature surrounding the meteor

In this section we estimate the gas temperature surrounding the meteor by means of the ionization degree of the plasma. It is well-known that the relative intensity of the spectrum lines are proportional to their relative densities as:

$$I_i = C \cdot N_i \cdot A_i \cdot h \cdot \nu_i \tag{1}$$

where, for each line of the spectrum, I_i is the relative emission intensity of an atomic or ionic species in the i-th state of ionization, C is a constant, A_i is the Einstein's coefficient in s^{-1} accounting for the probability of spontaneous emission between a given atom or ion excited electronic state and a lower energy state, ν_i is the

Table 5
Identified lines over 2-sigma and 3-sigma. Lines over 3-sigma are given in bold typeface. If blended lines, the strongest feature is given.

Wavelength (nm)			Σ intensity (A.U.)	
Measured	Theory	Identification	Measured	Blend
710.3	710.291	Zr I	0.09361	710.372 (Zr I) 710.448 (W I) 710.486 (W I) 710.526 (W I)
734.3	734.4695	Ti I	0.08957	734.396 (Zr I) 734.394 (Fe I) 734.449 (W I)
740.7	740.7821	O II	0.09131	740.837 (Fe II)
743.8	743.95532	Fe II	0.09312	743.719 (W I)
746.0	746.036	Fe I	0.1143	745.927 (W I) 746.219 (W I) 746.231 (Cr I)
746.6	**746.831**	**N I**	**0.1893**	**746.578 (Fe I)** **746.611 (W I)** **746.757 (Zr I)** **746.774 (W I)** **746.822 (W I)** **746.994 (Ti I)** **747.041 (W I)**
769.2	769.3254	Ti I	0.09693	
773.5	773.57981	Fe II	0.08958	773.629 (W I) 773.767 (Fe I)
776.2	776.224	N II	0.1062	776.298 (Cr I) 776.397 (Pd I)
777.2	**777.194**	**O I**	**1**	**777.165 (W I)** **777.169 (Cr I)** **777.252 (W I)** **777.348 (Fe II)** **777.417 (O I)** **777.468 (W I)** **777.539 (O I)** **777.673 (W I)**

frequency of the transition between atomic or ionic electronic states in s^{-1}, h is the Planck's constant and N_i is the density of ground or excited atoms or ions in the i-th state of ionization. We have identified two nitrogen lines in the meteor spectrum, corresponding to different ionization stages. If we consider that the main contributions are due only to nitrogen, then we can calculate an approximate value of the ionization degree of the plasma for each frame. We define the ionization degree as:

$$\frac{N_{i+1}}{N_{i+1}+N_i} = \frac{1}{1+\frac{I_i \cdot A_{i+1} \cdot \nu_{i+1}}{I_{i+1} \cdot A_i \cdot \nu_i}} \tag{2}$$

where I_i is the relative emission intensity of the N I line at 746.831 nm, and I_{i+1} is the relative emission intensity of the N II line at 776.224 nm. The values of I_i and I_{i+1} vary within the frame, so we have calculated the rate I_{i+1}/I_i and the ionization degree for each frame, as shown in the second column of Table 6.

If we consider the gas to be in thermal equilibrium – at least locally – so that the electron and gas temperatures have similar values ($T_e = T$), we can calculate the ionization degree of the plasma using the Saha equation:

$$\frac{n_e \cdot N_{i+1}}{N_i} = \frac{g_e \cdot g_{i+1} \cdot (2\pi m_e k_B T_e)^{3/2}}{g_i \cdot h^3} e^{\frac{-\chi_i}{k_B T_e}} \tag{3}$$

where n_e is the electron density, N_i is the density of ground or excited atoms or ions in the i-th state of ionization, g_i is the degeneracy or multiplicity of the considered atom or ion excited states, being $g_e = 2$, m_e is the mass of an electron, χ_i is the energy needed to ionize an atom in the ground state or in a given excited state. For N I in the excited state with excitation energy 11.99 eV (connected to the transition 746.831 nm) the value of χ_i needed for its ionization is 2.54 eV, k_B is the Boltzmann constant; T is the temperature of the gas and h is the Planck's constant.

The ionization degree is defined then as a function of the electron density and the gas temperature:

$$\frac{N_{i+1}}{N_{i+1}+N_i} = \frac{1}{1+\frac{n_e \cdot g_i \cdot h^3}{g_e \cdot g_{i+1} \cdot (2\pi m_e k_B T_e)^{3/2}} e^{\frac{-\epsilon_{i+1}+\epsilon_i}{k_B T_e}}} \tag{4}$$

being ϵ_i and ϵ_{i+1} the energies of the states i and $i+1$. Considering that the electron density could never exceed the gas density at a known altitude, we can calculate an upper limit of the electron temperature for a given ionization degree and altitude. The gas density at altitudes between 99.6 and 107.6 km is between $1.2322 \cdot 10^{13}$ cm^{-3} and $3.0208 \cdot 10^{12}$ cm^{-3} (Marsh et al., 2013); the corresponding maximum electron density is shown in the third column of Table 6. The fourth column of Table 6 is computed by solving Eq. (4) numerically for T; Fig. 5 plots the function in Eq. (4) for the electron density levels corresponding to 99.6–107.6 km altitude. According to Fig. 5 and Table 6, we found that the upper limit of the gas temperature surrounding the meteor was 1500 ± 100 K.

4. Discussion

4.1. Meteoroid source

The event discussed here was recorded during the activity period of the Orionids. It was registered about 5 days before the maximum of this meteor shower, which took place on October 21st at around 20:16 UT according to the International Meteor Organization [http://www.imo.net/live/orionids2014]. In order to validate the association of the progenitor meteoroid with the Orionid meteoroid stream, we have compared the orbit of this stream (Table 7 in Jenniskens (2006)) with the orbital data of the meteoroid listed in Table 4. This comparison has been performed, as usual, by calculating the value of the Southworth & Hawkins D_{SH} dissimilarity function (Southworth and Hawkins, 1963). This function measures the "distance" between both orbits (Williams, 2011). The computed value of D_{SH} yields 0.11, which is below the cut-off value of 0.15 usually adopted to establish a valid link (Lindblad, 1971a,b). This result confirms that the meteor belonged to the Orionid shower.

4.2. Photometric analysis

The lightcurve of the meteor is shown in Fig. 6.

As can be noticed, it exhibited no flares during its atmospheric path. This means that the meteoroid experienced a quasi-continuous fragmentation process without suffering any sudden disruption as it penetrated denser atmospheric regions. This smooth curve can be employed to calculate the initial (preatmospheric) mass m_∞ of the particle by means of the classical meteor luminous equation:

$$m = 2\int_{t_e}^{t_b} \frac{I}{\tau v^2} dt \tag{5}$$

in (5) I is the time-dependent luminosity of the meteor, which is related to its absolute magnitude M by means of the equation

$$I = 10^{-0.4 \times M} \tag{6}$$

The parameters t_b and t_e are the times corresponding to the beginning and the end of the luminous path, respectively, and τ is the luminous efficiency (i.e., the fraction of the kinetic energy of the

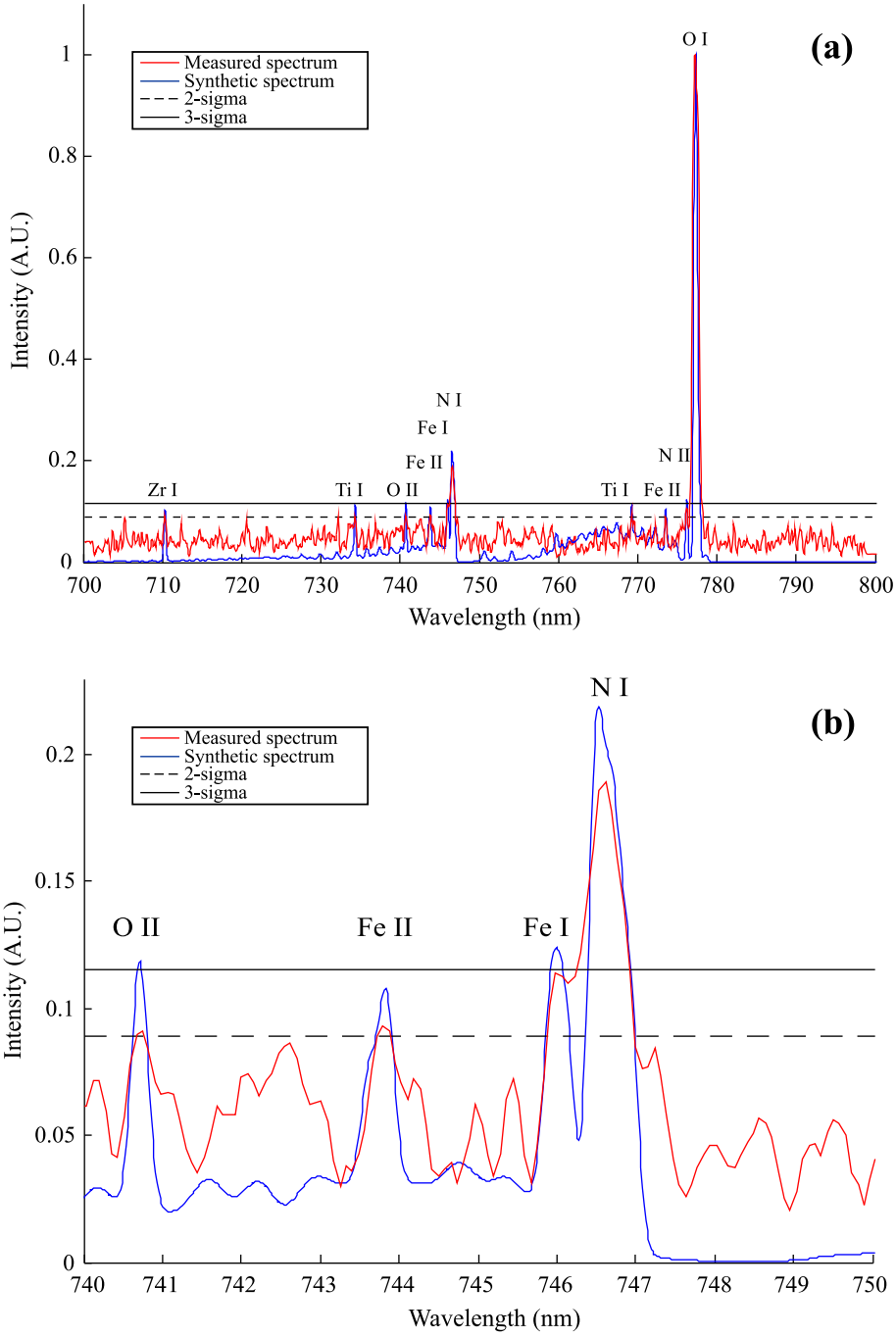

Fig. 4. Details of a meteor spectrum (red line) from 700 to 800 nm (a) and from 740 to 750 nm (b), obtained with GRASSP spectrograph on 2014 October 16th at 01:19:40 UT. Flux is dimensionless. The blue line is a composition of a N_2 first positive system synthetic spectrum at $T_{rot} = T_{vib} = T = 1500$ K, at an altitude between 99 and 108 km, combined with a synthetic spectrum of N I, N II, O I, Ti I, Cr I, Fe I, Fe II, Zr I, Pd I and W I atomic lines convolved with a gaussian curve of sigma 0.10 nm. Notice that the strongest features of N I at 742.364 and 744.229 nm cannot be found, although atomic lines of Fe have been identified. (For interpretation of the references to color in this figure legend, the reader is referred to the web version of this article.)

Table 6
Altitude, ionization degree, electron density and gas temperature estimated for each frame of the meteor spectrum video.

Altitude (km)	Ionization degree	$n_e(max)$ (cm^{-3})	$T_{gas}(max)$ (K)
107.6 ± 0.5	0.5442	$3.0208 \cdot 10^{12}$	1594.6911
105.6 ± 0.5	0.4752	$4.3034 \cdot 10^{12}$	1600.8048
103.6 ± 0.5	0.2443	$6.1298 \cdot 10^{12}$	1547.9219
101.6 ± 0.5	0.3566	$8.7046 \cdot 10^{12}$	1618.1201
99.6 ± 0.5	0.2637	$1.2322 \cdot 10^{13}$	1610.6464

meteoroid that is converted into light during the ablation process). This efficiency has been estimated by employing the relationships given by Ceplecha and McCrosky (1976). In this way, we have obtained that $m_\infty = 0.23 \pm 0.03$ g. If spherical shape is assumed for this particle and by taking into account the average bulk density $d = 0.9$ g cm^{-3} obtained for Orionid meteoroids (Babadzhanov and Kokhirova, 2009), the diameter of the meteoroid yields 0.78 ± 0.04 cm.

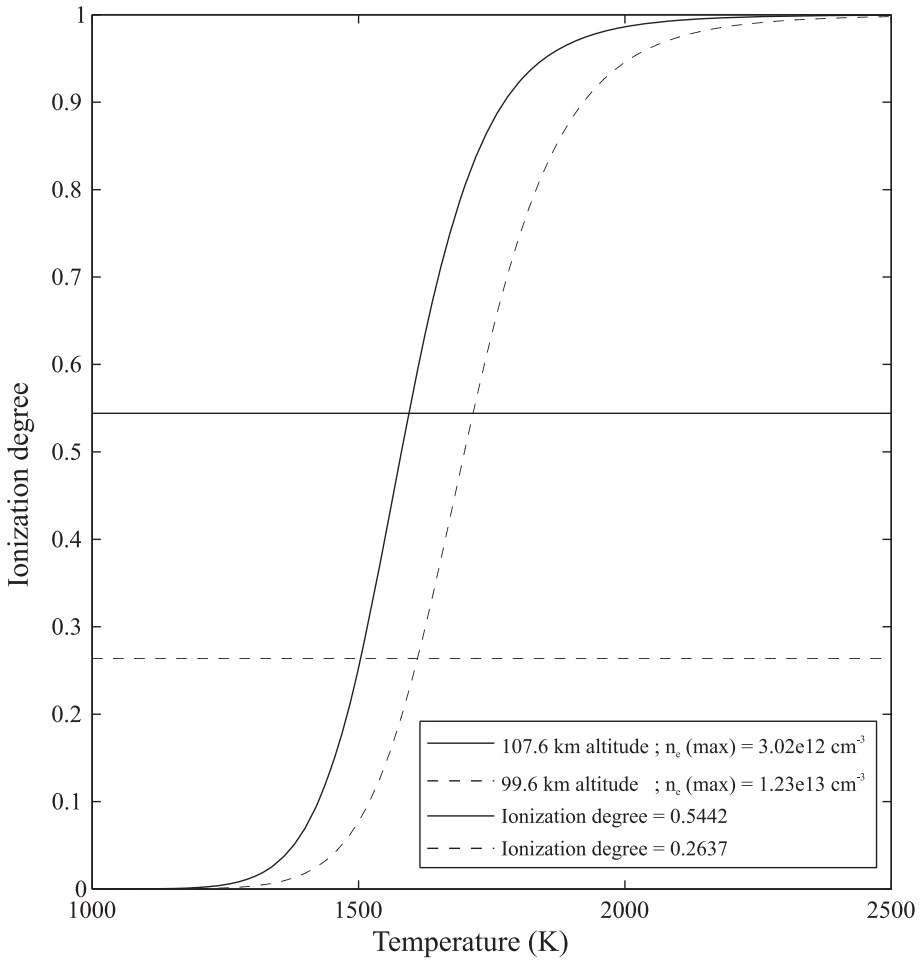

Fig. 5. Gas temperature calculated as a function of a given ionization degree and altitude. Dashed lines correspond to the ionization degree of the gas at 99.6 km altitude. Solid lines correspond to the ionization degree of the gas at 107.6 km altitude.

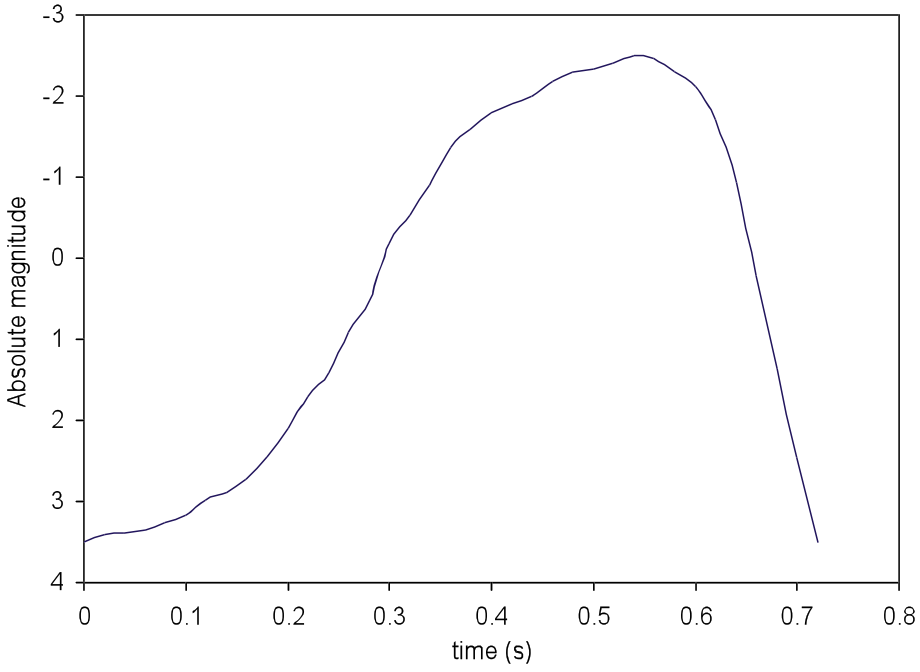

Fig. 6. Lightcurve (absolute magnitude vs. time) of the Orionid meteor analyzed in the text.

5. Summary and conclusions

We have analyzed a high resolution emission spectrum of a magnitude -2.5 ± 0.5 meteor serendipitously recorded by the GRASSP instrument on 2014 October 16th. The signal covers the wavelength range between 700 and 800 nm. The triangulation of the event has provided its atmospheric path and radiant, and the orbital elements of the progenitor meteoroid were also obtained. These data reveal that the particle belonged to the Orionid meteoroid stream.

In the spectrum, which has a resolution of 0.07 nm/pixel, we have identified the contributions of the atmospheric species N I, N II and O I. The emission of meteoroid species Ti I, Cr I, Fe I, Fe II, Zr I, Pd I and W I was also identified above the 2-sigma level. An upper limit of around 1500 K has been obtained for the gas temperature surrounding the meteor.

Acknowledgments

This work was supported by the Spanish Ministry of Science and Innovation, MINECO under projects ESP2013-48032-C5-5-R and FIS2014-61774-EXP and by the EU through the FEDER program.

References

Anderson, G.P. et al., 1993. Proc. SPIE Int. Soc. Opt. Eng. SPIE1968, p. 514. http://dx.doi.org/10.1117/12.154854.

Babadzhanov, P.B., Kokhirova, G.I., 2009. Densities and porosities of meteoroids. Astron. Astrophys., 353–358 http://dx.doi.org/10.1051/0004-6361:200810460.

Borovicka, J., 1993. A fireball spectrum analysis. Astron. Astrophys., 627–645.

Borovicka, J., 1994. Line identifications in a fireball spectrum. Astron. Astrophys. Suppl., 83–86.

Ceplecha, Z., 1987. Geometric, dynamic, orbital and photometric data on meteoroids from photographic fireball networks. Astron. Inst. Czech., Bull., 222–234.

Ceplecha, Z., McCrosky, R.E., 1976. Fireball end heights – A diagnostic for the structure of meteoric material. J. Geophys. Res., 6257–6275 http://dx.doi.org/10.1029/JB081i035p06257.

Fantz, U., 2006. Basics of plasma spectroscopy. Plasma Sour. Sci. Technol., 137–147 http://dx.doi.org/10.1088/0963-0252/15/4/S01.

Gordillo-Vázquez, F.J., Luque, A., Simek, M., 2011. Spectrum of sprite halos. J. Geophys. Res.: Space Phys. 116, A09319. http://dx.doi.org/10.1029/2011JA016652.

Gordillo-Vázquez, F.J., Luque, A., Simek, M., 2012. Near infrared and ultraviolet spectra of TLEs. J. Geophys. Res.: Space Phys. 117, A05329. http://dx.doi.org/10.1029/2012JA017516.

Jenniskens, P., 2006. Meteor Showers and their Parent Comets. Cambridge University Press.

Jenniskens, P., 2007. Quantitative meteor spectroscopy: Elemental abundances. Adv. Space Res., 491–512 http://dx.doi.org/10.1016/j.asr.2007.03.040.

Jenniskens, P. et al., 2000. FeO Orange Arc emission detected in optical spectrum of Leonid persistent train. Earth Moon Planets, 429–438. http://dx.doi.org/10.1023/A:1017079725808.

Kramida, A. et al., 2014. NIST Atomic Spectra Database (ver. 5.2). National Institute of Standards and Technology, Gaithersburg, MD, <http://physics.nist.gov/asd> (23.06.15).

Lindblad, B.A., 1971a. A computerized stream search among 2401 photographic meteor orbits. Smithson. Contrib. Astrophys., 14–24 http://dx.doi.org/10.5479/si.00810231.12.14.

Lindblad, B.A., 1971b. A stream search among 865 precise photographic meteor orbits. Smithson. Contrib. Astrophys., 1–13.

Madiedo, J.M., 2014. Robotic systems for the determination of the composition of Solar System materials by means of fireball spectroscopy. Earth, Planets Space, 70–79. http://dx.doi.org/10.1186/1880-5981-66-70.

Madiedo, J.M., 2015. The ρ-Geminid meteoroid stream: Orbits, spectroscopic data and implications for its parent body. Mon. Not. R. Astron. Soc., 2135–2140 http://dx.doi.org/10.1093/mnras/stv148.

Madiedo, J.M., Trigo-Rodriguez, J.M., 2008. Multi-station video orbits of minor meteor showers. Earth Moon Planets, 133–139. http://dx.doi.org/10.1007/s11038-007-9215-x.

Madiedo, J.M. et al., 2013a. The 2011 October Draconids outburst – II. Meteoroid chemical abundances from fireball spectroscopy. Mon. Not. R. Astron. Soc., 571–580 http://dx.doi.org/10.1093/mnras/stt748.

Madiedo, J.M. et al., 2013b. The Northern χ-Orionid meteoroid stream and possible association with the potentially hazardous Asteroid 2008XM1. Mon. Not. R. Astron. Soc., 2464–2470 http://dx.doi.org/10.1093/mnras/stt342.

Madiedo, J.M. et al., 2013c. On the activity of the γ-Ursae Minorids meteoroid stream in 2010 and 2011. Mon. Not. R. Astron. Soc., 1678–1685 http://dx.doi.org/10.1093/mnras/stt288.

Marsh, D.R. et al., 2013. Climate change from 1850 to 2005 simulated in CESM1 (WACCM). Am. Meteorol. Soc. 26, 7372–7391. http://dx.doi.org/10.1093/mnras/stt288.

Parra-Rojas, F.C. et al., 2013. Spectroscopic diagnostics of laboratory air plasmas as a benchmark for spectral rotational (gas) temperature determination in TLEs. J. Geophys. Res.: Space Phys. 118, 4649. http://dx.doi.org/10.1002/jgra.50433.

Passas, M. et al., 2014. Transient upper atmospheric plasmas: Sprites and halos. IEEE Trans. Plasma Sci. 42, 2664–2665.

Southworth, Z., Hawkins, R.E., 1963. Statistics of meteor streams. Smithsonian Contrib. Astrophys., 261–261.

Trigo-Rodriguez, J.M. et al., 2009a. The outburst of the κ Cygnids in 2007: Clues about the catastrophic break up of a comet to produce an Earth-crossing meteoroid stream. Mon. Not. R. Astron. Soc., 367–375 http://dx.doi.org/10.1111/j.1365-2966.2008.14060.x.

Trigo-Rodriguez, J.M. et al., 2009b. Observations of a very bright fireball and its likely link with Comet C/1919 Q2 Metcalf. Mon. Not. R. Astron. Soc., 569–576 http://dx.doi.org/10.1111/j.1365-2966.2008.14363.x.

Williams, I.P., 2011. The origin and evolution of meteor showers and meteoroid streams. Astron. Geophys., 220–2.26. http://dx.doi.org/10.1111/j.1468-4004.2011.52220.x.